2D Materials

Magnetic proximity in a van der Waals heterostructure of magnetic insulator and graphene

To cite this article: Bogdan Karpiak *et al* 2020 *2D Mater.* **7** 015026

View the article online for updates and enhancements.

Recent citations

- Observation of charge to spin conversion in Weyl semimetal WTe2 at room temperature
  Bing Zhao *et al*

- Magnetic Proximity Effect in Graphene/CrBr 3 van der Waals Heterostructures
  Chaolong Tang *et al*

- Two-dimensional spintronic circuit architectures on large scale graphene
  Dmitrii Khokhriakov *et al*

2D Materials

PAPER

Magnetic proximity in a van der Waals heterostructure of magnetic insulator and graphene

Bogdan Karpiak[1], Aron W Cummings[2], Klaus Zollner[3], Marc Vila[2,4], Dmitrii Khokhriakov[1], Anamul Md Hoque[1], André Dankert[1], Peter Svedlindh[5], Jaroslav Fabian[3], Stephan Roche[2,6] and Saroj P Dash[1,7,8]

1 Department of Microtechnology and Nanoscience, Chalmers University of Technology, SE-41296, Göteborg, Sweden
2 Catalan Institute of Nanoscience and Nanotechnology (ICN2), CSIC and The Barcelona Institute of Science and Technology, Campus UAB, Bellaterra, 08193 Barcelona, Spain
3 Institute for Theoretical Physics, University of Regensburg, 93040 Regensburg, Germany
4 Department of Physics, Universitat Autònoma de Barcelona, Campus UAB, Bellaterra, 08193 Barcelona, Spain
5 Division of Solid-State Physics, Department of Engineering Science, Uppsala University, Box 534, SE-75121 Uppsala, Sweden
6 ICREA—Institució Catalana de Recerca i Estudis Avançats, 08010 Barcelona, Spain
7 Graphene Center, Chalmers University of Technology, SE-41296, Göteborg, Sweden
8 Author to whom any correspondence should be addressed.

E-mail: saroj.dash@chalmers.se

Abstract

Engineering 2D material heterostructures by combining the best of different materials in one ultimate unit can offer a plethora of opportunities in condensed matter physics. Here, in the van der Waals heterostructures of the ferromagnetic insulator $Cr_2Ge_2Te_6$ and graphene, our observations indicate an out-of-plane proximity-induced ferromagnetic exchange interaction in graphene. The perpendicular magnetic anisotropy of $Cr_2Ge_2Te_6$ results in significant modification of the spin transport and precession in graphene, which can be ascribed to the proximity-induced exchange interaction. Furthermore, the observation of a larger lifetime for perpendicular spins in comparison to the in-plane counterpart suggests the creation of a proximity-induced anisotropic spin texture in graphene. Our experimental results and density functional theory calculations open up opportunities for the realization of proximity-induced magnetic interactions and spin filters in 2D material heterostructures and can form the basic building blocks for future spintronic and topological quantum devices.

Introduction

Topological quantum states of matter and spintronics have considerable interest in the field of condensed matter physics for applications in low-power electronics without the application of an external magnetic field [1, 2]. The generation of magnetic exchange interaction and strong spin–orbit coupling in two-dimensional (2D) Dirac materials such as graphene is expected to result in the emergence of quantum anomalous Hall state and topologically protected chiral spin textures [3, 4]. Graphene, having excellent charge and spin transport properties, is a suitable atomically-thin 2D material to create proximity-induced effects when placed in heterostructures with other functional materials [5–7]. Proximity-induced magnetic effects have been investigated in 2D semiconductors on graphene in heterostructures with ferromagnetic semiconductors [8] and magnetic oxides [9–16]. However, there are severe challenges in producing a sizable out-of-plane exchange interaction in magnetic oxide-graphene structures due to the in-plane magnetic anisotropy of the oxide-based magnetic insulators used so far with graphene [13].

To create significant proximity-induced magnetic interaction in graphene, the use of a magnetic insulator with perpendicular magnetic anisotropy is desired. Additionally, for a good interface, atomically-flat layered 2D material-based van der Waals heterostructures (vdWh) are ideal [1–4]. Recently, 2D magnetic materials were successfully prepared

via exfoliation down to the monolayer limit, showing intrinsic long-range Heisenberg ferromagnetic order [17–19] that is tunable by application of a gate voltage [20–22]. Additionally, giant tunneling magnetoresistance, spin filtering and magnon-assisted tunneling phenomenon have been demonstrated using such 2D magnetic materials [23–27]. Recently, heterostructures of such 2D magnetic materials with 2D semiconductors [8], topological insulators [28], semimetals [29] and graphene [27] have also been investigated. Theoretical predictions indicate that heterostructures of 2D magnetic insulators with graphene are expected to produce a large exchange splitting in the graphene layer, enabling the emergence of a topological quantum phase [30–32].

Here, we use van der Waals heterostructures of graphene with the ferromagnetic insulator $Cr_2Ge_2Te_6$ (CGT) having a perpendicular magnetic anisotropy to demonstrate a proximity-induced magnetic exchange interaction, which is revealed by the temperature-dependent splitting of Hanle spin precession signals. The observed anisotropic spin relaxation indicates a possible nontrivial spin texture imprinted in graphene by proximity to CGT. The demonstration of out-of-plane proximity-induced magnetism induced in graphene is a crucial step towards realizing more exotic electronic states in 2D material heterostructures.
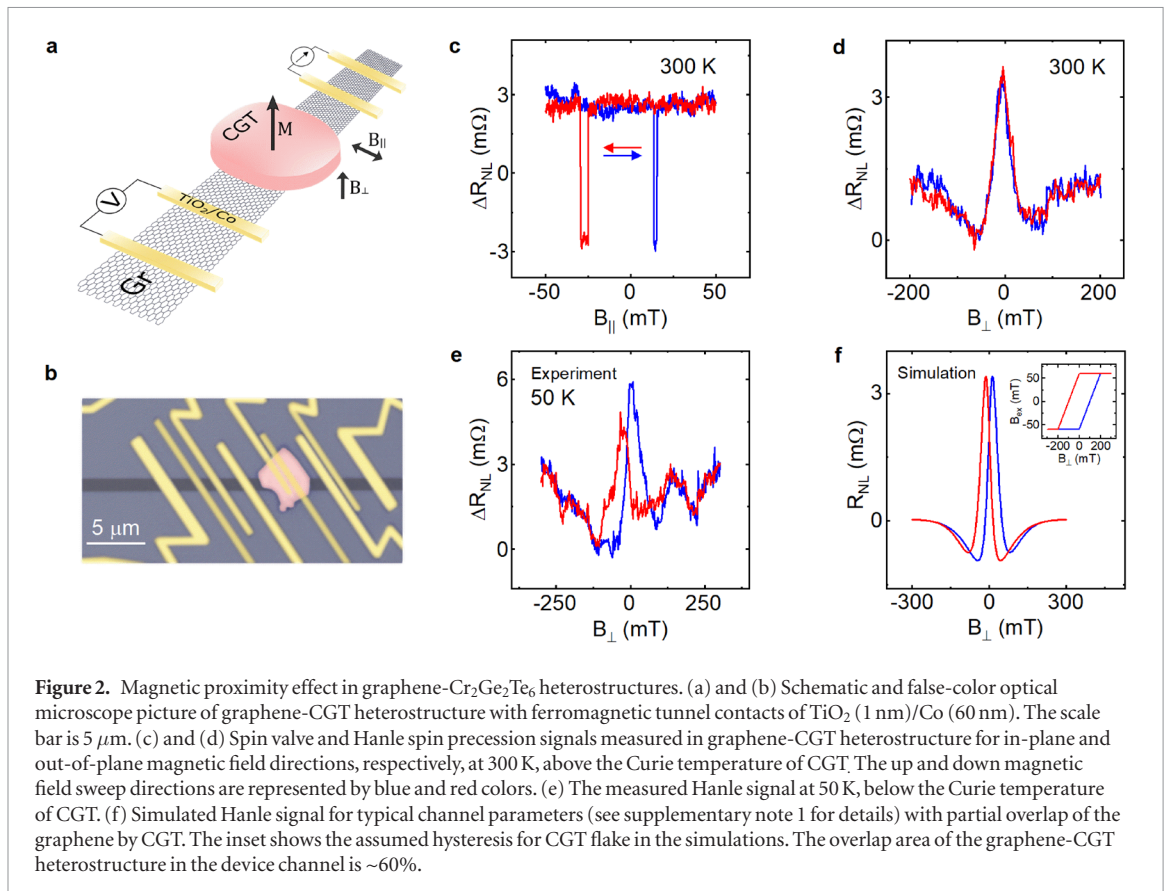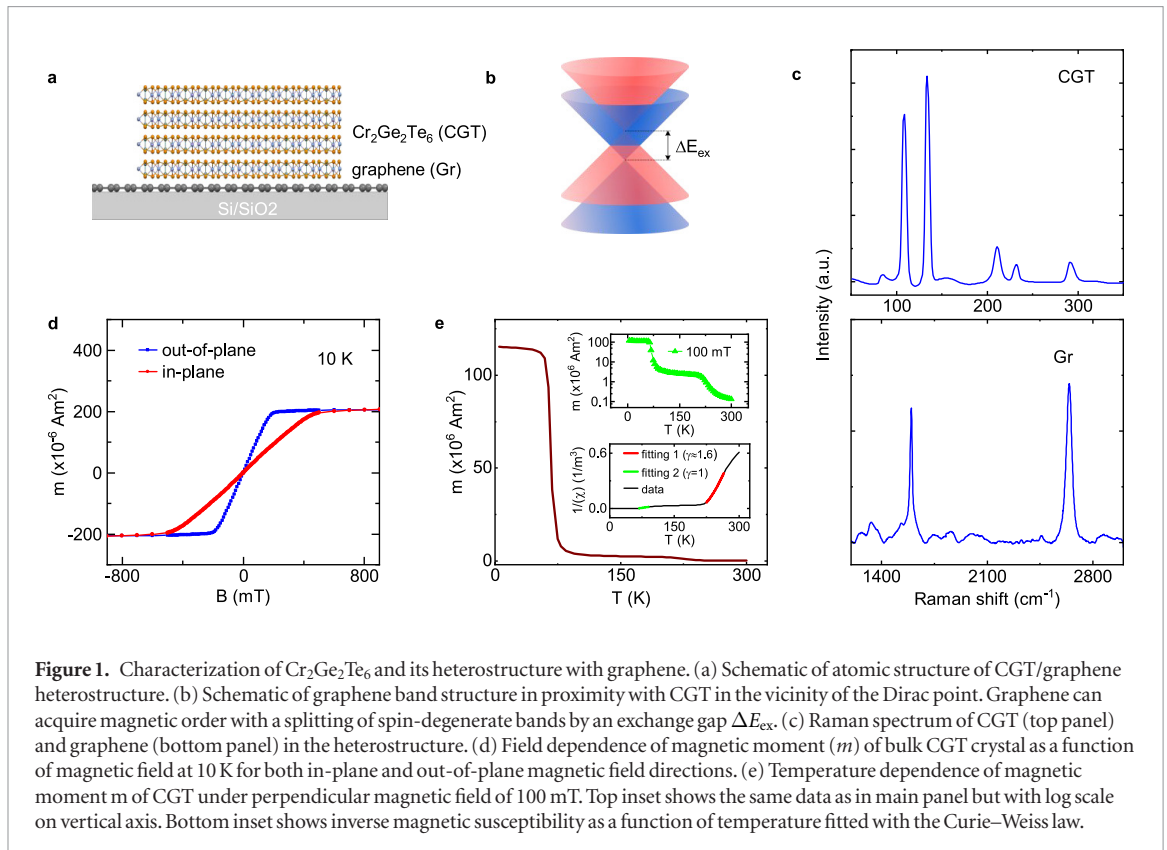
Results

The van der Waals heterostructures are prepared by dry-transferring CGT flakes (~ 30 nm in thickness) onto chemical vapor deposited (CVD) graphene on a SiO_2/n-Si substrate in a cleanroom environment within one minute after exfoliation. The atomic structure of the CGT flakes consists of van der Waals layers of Cr atoms sandwiched by Te and Ge atoms with an interlayer distance of ~ 6.9 Å (figure 1(a)) [33, 34]. The choice of CGT is motivated by its layered structure, insulating behavior [30, 35], and perpendicular magnetic anisotropy [17]. CGT is expected to induce a magnetic exchange interaction in graphene, splitting the spin-degenerate graphene bands by a characteristic exchange ΔE_{ex} (figure 1(b)). The Raman spectrum of the CGT flake in a heterostructure with graphene is shown in figure 1(c). It contains the phonon mode at $108\,cm^{-1}$, which is characteristic of a CGT flake with more than one layer [36]. We do not observe any broad peak at $121\,cm^{-1}$, characteristic of an oxidized CGT surface (supplement figure S1 (stacks.iop.org/TDM/7/015026/mmedia)) after long exposure to the ambient atmosphere, indicating absence of substantial oxidation in freshly cleaved CGT flakes. The Raman spectrum of the CVD deposited graphene channel (figure 1(c)) contains a 2D peak ($2642\,cm^{-1}$) of stronger intensity than the G peak ($1600\,cm^{-1}$), indicating monolayer thickness of graphene [37]. Magnetic characterization of the bulk CGT crystal by SQUID magnetometry shows

perpendicular magnetic anisotropy of the material (figure 1(d)). From the temperature dependence of the magnetization of the bulk CGT crystal under a perpendicularly applied magnetic field of 100 mT (figure 1(e)), one can observe two magnetic ordering temperatures. By fitting the inverse magnetic susceptibility according to the Curie–Weiss law $\frac{1}{\chi} = \frac{(T-Tc)^\gamma}{C}$ (inset in figure 1(e)), values of the transition temperatures of ~65 K ($\gamma = 1$) and ~204 K ($\gamma \approx 1.6$) were obtained. The former shows a more distinct magnetization enhancement with deceasing temperature. The magnetic moment *m* of the high temperature ($T_c \sim 204$ K) phase is, however, two orders of magnitude smaller than that of the main magnetic phase ($T_c \sim 65$ K). The presence of a magnetic transition at higher temperature (figure 1(e) and supplement figure S2) could be due to imperfections in the lattice structure or an extra magnetic phase leading to a magnetic transition at higher temperature in the regions of the material with broken stoichiometry and lattice defects.

Magnetic proximity effect in graphene-$Cr_2Ge_2Te_6$ heterostructures
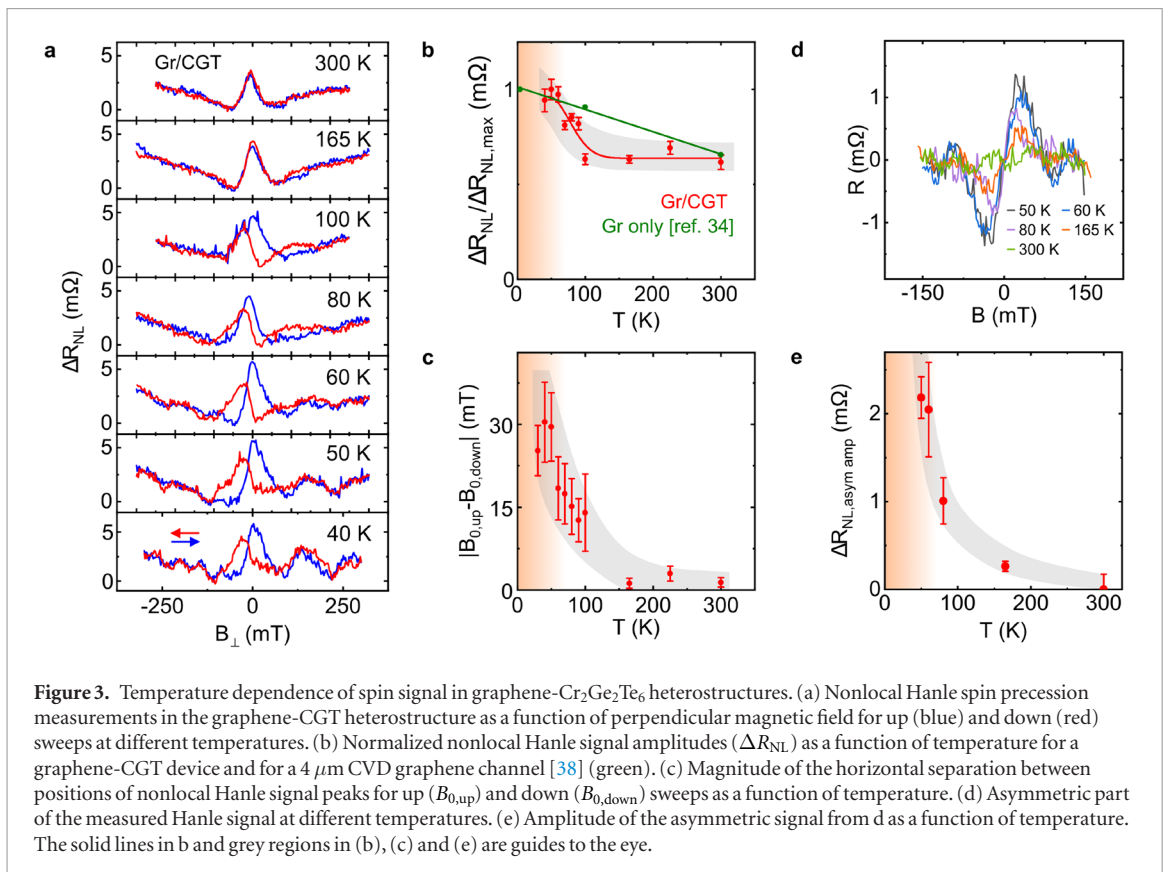
The device schematic and an optical microscope image of a nanofabricated device consisting of a graphene–CGT heterostructure channel are shown in figures 2(a) and (b) (see methods for details about the device fabrication process). The ferromagnetic tunnel contacts of Co/TiO_2 on graphene are used for injection and detection of the spin-polarized current in the heterostructure channel, with three-terminal contact resistances of 3–6 kΩ at room temperature (supplement figure S3). In such graphene-CGT heterostructure devices, we probe the proximity-induced exchange interaction by employing spin transport and Hanle precession measurements. The insulating behavior of CGT (two-terminal resistance ~ 60 MΩ) allows charge carriers to flow mostly in the graphene layer with a field-effect mobility of ~2400 cm^2 V^{-1} s^{-1} in the heterostructure channel (supplement figure S4).

First, spin-valve and Hanle precession measurements were carried out at room temperature (300 K), well above the T_c of CGT, to check the functionality of the heterostructure devices in a nonlocal (NL) configuration (see figure 2(a)). A NL spin resistance change $\Delta R_{NL} = \Delta V_{NL}/I \approx 5.5$ mΩ was measured at 300 K while sweeping the in-plane magnetic field ($B_\parallel$) along the easy axis of the Co contacts in a device with channel length $L = 6.9\,\mu$m (figure 2(c)). Next, Hanle measurements were conducted in the NL configuration but with an out-of-plane applied magnetic field ($B_\perp$), which causes in-plane Larmor precession of spins as they propagate through the heterostructure channel. Such measurements at room temperature (figure 2(d)) for both up and down magnetic field sweeps showed conventional Hanle signals without any special features [38]. By fitting the data with the

Figure 1. Characterization of $Cr_2Ge_2Te_6$ and its heterostructure with graphene. (a) Schematic of atomic structure of CGT/graphene heterostructure. (b) Schematic of graphene band structure in proximity with CGT in the vicinity of the Dirac point. Graphene can acquire magnetic order with a splitting of spin-degenerate bands by an exchange gap ΔE_{ex}. (c) Raman spectrum of CGT (top panel) and graphene (bottom panel) in the heterostructure. (d) Field dependence of magnetic moment (m) of bulk CGT crystal as a function of magnetic field at 10 K for both in-plane and out-of-plane magnetic field directions. (e) Temperature dependence of magnetic moment m of CGT under perpendicular magnetic field of 100 mT. Top inset shows the same data as in main panel but with log scale on vertical axis. Bottom inset shows inverse magnetic susceptibility as a function of temperature fitted with the Curie–Weiss law.

Figure 2. Magnetic proximity effect in graphene-$Cr_2Ge_2Te_6$ heterostructures. (a) and (b) Schematic and false-color optical microscope picture of graphene-CGT heterostructure with ferromagnetic tunnel contacts of TiO_2 (1 nm)/Co (60 nm). The scale bar is 5 μm. (c) and (d) Spin valve and Hanle spin precession signals measured in graphene-CGT heterostructure for in-plane and out-of-plane magnetic field directions, respectively, at 300 K, above the Curie temperature of CGT. The up and down magnetic field sweep directions are represented by blue and red colors. (e) The measured Hanle signal at 50 K, below the Curie temperature of CGT. (f) Simulated Hanle signal for typical channel parameters (see supplementary note 1 for details) with partial overlap of the graphene by CGT. The inset shows the assumed hysteresis for CGT flake in the simulations. The overlap area of the graphene-CGT heterostructure in the device channel is ~60%.

solution of the Bloch equation that describes spin dynamics in the channel with an applied $B_\perp$ [38], the spin lifetime $\tau_s = 244 \pm 32$ ps, diffusion coefficient $D_s = 0.019 \pm 0.005$ m^2 s^{-1} and diffusion length $\lambda = 2.1 \pm 0.4$ μm were obtained.

At low temperatures (50 K), below the Curie point of CGT (figure 2(e)), one can notice two distinctive features of the measured Hanle signal: a shift of the two Hanle peaks with respect to each other and asymmetry of the Hanle peak. Such observations are indicative of

Figure 3. Temperature dependence of spin signal in graphene-$Cr_2Ge_2Te_6$ heterostructures. (a) Nonlocal Hanle spin precession measurements in the graphene-CGT heterostructure as a function of perpendicular magnetic field for up (blue) and down (red) sweeps at different temperatures. (b) Normalized nonlocal Hanle signal amplitudes (ΔR_{NL}) as a function of temperature for a graphene-CGT device and for a 4 μm CVD graphene channel [38] (green). (c) Magnitude of the horizontal separation between positions of nonlocal Hanle signal peaks for up ($B_{0,up}$) and down ($B_{0,down}$) sweeps as a function of temperature. (d) Asymmetric part of the measured Hanle signal at different temperatures. (e) Amplitude of the asymmetric signal from d as a function of temperature. The solid lines in b and grey regions in (b), (c) and (e) are guides to the eye.

an out-of-plane magnetism induced in the graphene by proximity to CGT. These features are also seen in simulations (figure 2(f) and supplementary note 1) obtained from the solution of the Bloch equation that considers a magnetic exchange interaction in graphene due to the influence of the CGT flake [39]. The CGT flake can induce ferromagnetism in the underlying graphene via the exchange field B_{ex}, which adds to the external magnetic field, $B_\perp \rightarrow B_\perp + B_{ex} + B_s$, and thus modifies the Hanle spin precession signal in the heterostructure channel. While the stray fields B_s do contribute to the spin precession in the channel in a similar way as B_{ex}, the observed Hanle signals are mainly shaped by the contributions from externally applied and exchange fields (see supplementary note 2). The peak splitting between the two Hanle sweeps can then originate from hysteretic behavior [20] of the proximity-induced magnetic exchange fields in graphene. This alters the position of the Hanle peak corresponding to zero total field, which, due to hysteresis, is obtained at different values of the applied magnetic field depending on the sweep direction.

Meanwhile, the asymmetry of the Hanle peak arises from the spatial inhomogeneity of the proximity-induced exchange field; a finite graphene-CGT interfacial region leads to an asymmetry, while CGT covering the entire graphene flake would result in a symmetric Hanle curve (see supplementary note 1). Since hysteresis gives opposite shifts of the exchange field depending on the sweep direction, this is reflected in the opposite asymmetry of the measured Hanle signals (figures 2(e) and (f)). The measurements in the

two devices with different CGT/graphene channel overlaps by the CGT flake confirm decreased asymmetry with increased channel overlap (supplementary note 3), which is in agreement with simulation results (supplementary note 1).

To further elucidate the proximity-induced magnetic interaction in graphene-CGT heterostructures, the Hanle spin precession measurements were performed at several different temperatures in a systematic manner (figure 3(a)). The measured data reveal a rapid decrease of the nonlocal spin signal amplitude (R_{NL}) with increasing temperature in comparison to the temperature dependence of pristine graphene (figure 3(b)) [38], followed by a saturation of the signal above the curie temperature of the CGT. The rapid spin signal amplitude decay with temperature in the range of $T < T_c$, compared to pristine graphene [38], can be attributed to fluctuating proximity-induced magnetic exchange fields due to random fluctuations of the magnetization of the CGT flake, which become more pronounced approaching the magnetic ordering temperature of CGT [15]. Such fluctuations cause random changes of the proximity-induced exchange field and, hence, the effective field that acts on the propagating spins, leading to enhanced spin relaxation [40, 41]. Furthermore, the separation between the peaks for opposite Hanle sweeps vanishes at elevated temperatures (figure 3(c)).

The presence of Hanle peak shifts indicates that the proximity-induced exchange field in graphene persists above the Curie temperature for bulk CGT [28] (~ 65 K) up to at least 100 K. Additionally, one can deconvolute

the measured Hanle signal into symmetric and asymmetric components, where the latter contains information on additional rotation of spins in the channel [42] with respect to normal precession caused by the applied perpendicular magnetic field. Such rotation can originate e.g. from the modified spin texture of graphene under the CGT flake caused by the proximity to the latter. From figures 3(d) and (e) one can see that the asymmetric contribution to the signal also vanishes with increasing temperature in a comparable way as in figure 3(c). This suggests the same origin for peak splitting and asymmetry—both can arise from the proximity-induced exchange field in the graphene channel under the flake, which persists at $T > T_c$ of bulk CGT and decays with increasing temperature, while being completely absent at temperatures above 165 K. Fitting the symmetric component of the Hanle signal with the solution of the Bloch equation for spin diffusion in a homogeneous channel gives values of the in-plane spin lifetimes $\tau_{||}$ in the range of 90–280 ps; the comparably large spread of values results due to a large number of free fitting parameters (see supplementary note 4). However, most fits resulting in reasonable spin transport parameters yielded an exchange field on the order of a few 10s of mT.
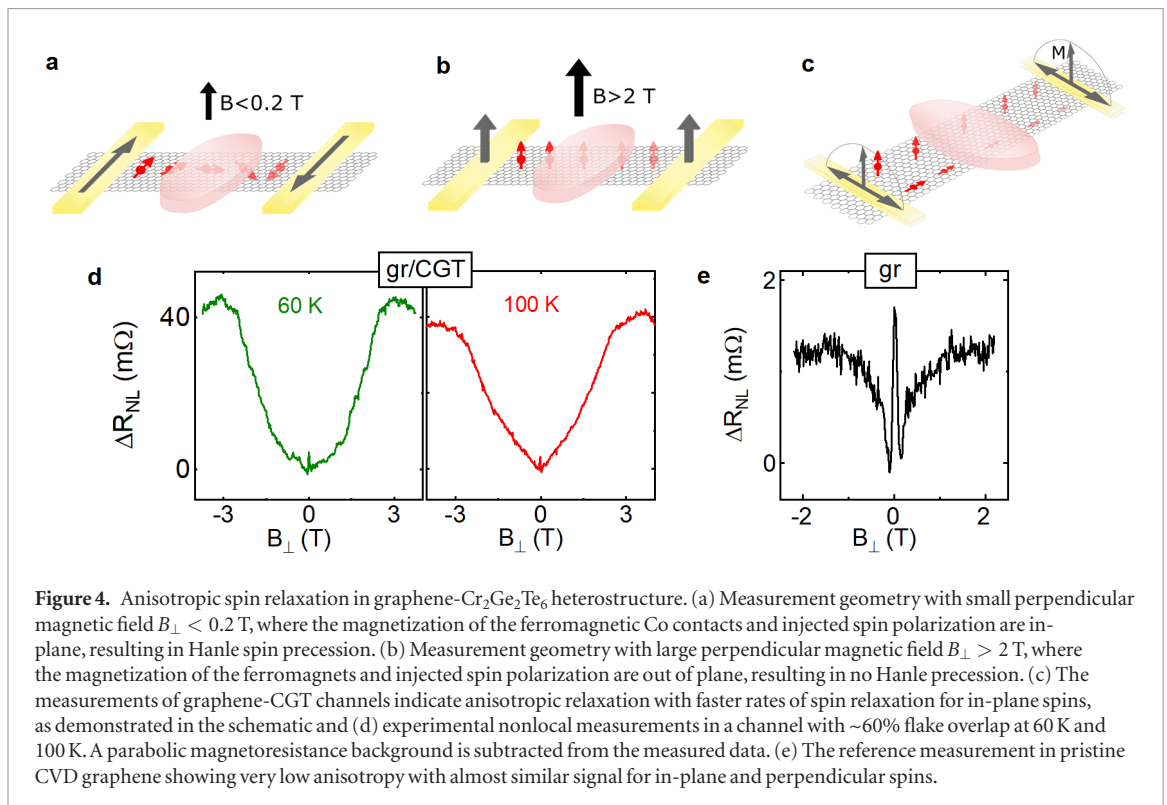
Anisotropic spin relaxation in graphene-CGT insulator heterostructures

The proximity-induced exchange interactions in the graphene-based heterostructures can also result in spin relaxation anisotropy. Here we observe spin relaxation anisotropy in graphene-CGT heterostructures by employing the same NL Hanle measurement configuration. However, here the field sweep range is broader, allowing the injection and detection of both in-plane and out-of-plane spins in different field ranges. In-plane spins are injected and detected at low field values when the contacts are magnetized in-plane at magnetic fields $B_\perp < 0.4$ T (figure 4(a)). With increasing out-of-plane field the magnetization of the contacts starts to rotate to the out-of-plane direction, reaching saturation at $B_\perp > 2$ T (figure 4(b)). When spins relax with different rates in the in-plane or out-of-plane direction, different amplitudes of the signal are observed for the corresponding magnetic field ranges (figure 4(c)). Therefore, the in-plane spin lifetime $\tau_{||}$ is estimated from low $B_\perp$-field Hanle data, while the out-of-plane spin lifetime $\tau_\perp$ is extracted from large out-of-plane $B_\perp$-field measurements. As shown in figure 4(d), in the graphene-CGT heterostructure the spin signal magnitudes at $B_\perp = 0$ for in-plane spins ($\Delta R_{NL}^{||}$) and at $B_\perp = 2.5$ T for spins perpendicular to plane ($\Delta R_{NL}^\perp$) show strong anisotropy, with $\Delta R_{NL}^\perp > \Delta R_{NL}^{||}$ and with a ratio $\Delta R_{NL}^\perp / \Delta R_{NL}^{||} \sim 10$. The spin lifetime anisotropy $r \equiv \tau_\perp / \tau_{||}$ is obtained from $\Delta R_{NL}^\perp / \Delta R_{NL}^{||} = \sqrt{r} e^{-(L/\lambda_{||})(\frac{1}{\sqrt{r}} - 1)}$, where L is the channel length and $\lambda_{||}$ is the spin diffusion length

for in-plane spins [43]. From this expression we find a strong anisotropy, with $\tau_\perp$ being 3.9 times the value of $\tau_{||} \sim 150$ ps (assuming homogeneous channel characteristics). Such observations are in contrast with the isotropic spin relaxation in pristine graphene channels, which have a value of r close to 1 (0.94±0.01 in figure 4(e)).

The observed anisotropic spin relaxation in graphene-CGT heterostructures could occur, for example, if spin relaxation is dominated by the so-called valley-Zeeman spin–orbit coupling (SOC), similar to the case of graphene on transition metal dichalcogenides [44, 45]. Valley-Zeeman SOC (λ_{VZ}) generates an out-of-plane spin texture that, in the presence of strong inter-valley scattering (τ_{iv}), quickly relaxes the in-plane spins and results in large anisotropy. To determine the type and magnitude of SOC induced in graphene by CGT, we perform density functional theory (DFT) simulations of the graphene-CGT heterostructure (see methods and supplementary note 5). By evaluating the band splitting at both K and K' valleys, we obtain a Rashba SOC $\lambda_R = 0.253$ meV and $\lambda_{VZ} = 0.113$ meV. Assuming $\tau_{iv} = (5 - 10)\,\tau_p$, where τ_p is the momentum scattering time, we obtain an anisotropy of the order $r = (\lambda_{VZ}/\lambda_R)^2 (\tau_{iv}/\tau_p) + 1/2 = 1.5$–2.5.

While SOC can induce a spin lifetime anisotropy $r > 1$, the temperature dependence of the spin signal in figure 3(b) suggests that magnetic exchange fluctuations are playing a role in the spin relaxation. In this scenario, an apparent spin relaxation anisotropy can also emerge. In case of the exchange fluctuation mechanism the spins are dephased by the fluctuations, but if magnetic field is applied the fluctuations are suppressed. This is different for spins parallel and perpendicular to the applied magnetic field, which results in an increase of anisotropy with increasing out-of-plane magnetic field $B_\perp$. Assuming that exchange fluctuations are the sole source of spin relaxation in the graphene-CGT devices, we find that the spin relaxation is nearly completely isotropic ($r \approx 1.002$) at $B_\perp = 0$ and becomes anisotropic with increasing values of $B_\perp$ (see supplementary note 6). This analysis indicates that if the spin relaxation is dominated by exchange fluctuations, the large anisotropy seen in figure 4(d) can be driven by the external field $B_\perp$ and may not be intrinsic to the graphene/CGT interface. This is because the perpendicular proximity-induced exchange field B_{ex}, while sufficiently large to see in Hanle measurements, is not large enough to suppress exchange fluctuations in graphene. It is still unclear whether spin relaxation is dominated by SOC, exchange fluctuations, or a combination of the two. However, considering that according to DFT calculations the exchange splitting is expected to be an order of magnitude stronger than SOC (see discussion for supplement figure S10), one can expect the origin of the experimentally observed anisotropy of spin relaxation to be mainly caused by the exchange fluctuations. Figure 3(b) points to at least some contribution of exchange fluctuations, while

Figure 4. Anisotropic spin relaxation in graphene-Cr$_2$Ge$_2$Te$_6$ heterostructure. (a) Measurement geometry with small perpendicular magnetic field $B_\perp < 0.2$ T, where the magnetization of the ferromagnetic Co contacts and injected spin polarization are in-plane, resulting in Hanle spin precession. (b) Measurement geometry with large perpendicular magnetic field $B_\perp > 2$ T, where the magnetization of the ferromagnets and injected spin polarization are out of plane, resulting in no Hanle precession. (c) The measurements of graphene-CGT channels indicate anisotropic relaxation with faster rates of spin relaxation for in-plane spins, as demonstrated in the schematic and (d) experimental nonlocal measurements in a channel with ~60% flake overlap at 60 K and 100 K. A parabolic magnetoresistance background is subtracted from the measured data. (e) The reference measurement in pristine CVD graphene showing very low anisotropy with almost similar signal for in-plane and perpendicular spins.

the anisotropy measurement in figure 4(d) can be explained by either of the mechanisms.

Summary and outlook

In summary, the observed modulation of the spin transport signal demonstrates the existence of an exchange interaction in graphene proximity-coupled to the layered magnetic insulator CGT. This is revealed by the observation of nontrivial features in the measured nonlocal Hanle spin precession signals in the graphene-CGT channel. Namely, at low temperatures there is a hysteretic shift of the Hanle signal maxima for opposite magnetic field sweep directions, accompanied by a corresponding asymmetry in the Hanle signal. These features persist up to at least 100 K, above the T_c of bulk CGT. Supporting simulations reveal that these features can be explained by out-of-plane magnetism induced in the graphene layer by CGT. Additionally, measurements of large spin lifetime anisotropy indicate that proximity coupling of the graphene channel to CGT can modify its spin texture. This anisotropy can arise from the magnetic exchange induced in the graphene, while DFT simulations suggest that spin–orbit coupling could also be playing a role. Looking ahead, the proximity-induced effects can be further tuned by tailoring the van der Waals gap between graphene and CGT [30], and by placing it on both sides of the graphene layer. These achievements are important for the realization of quantum states of matter characterized by edge states which are topologically protected from backscattering without the application of an external magnetic field, namely, the quantum anomalous Hall effect [30–32]. This

holds great potential for applications in spintronics and low-power quantum electronics.

Methods

Device fabrication and measurement
To fabricate the devices, CVD graphene was wet-transferred onto a Si/SiO$_2$ substrate (from Graphenea). After patterning the graphene into stripes of typical lateral width of 1–4 μm by photolithography and annealing in an Ar/H$_2$ atmosphere, 2D flakes (~30 nm thick) of the hexagonal ferromagnetic insulator Cr$_2$Ge$_2$Te$_6$ (from HQ Graphene), prepared by exfoliation method, were dry transferred immediately to reduce oxidation from air exposure. Suitable graphene-CGT heterostructure areas were chosen by optical microscope for further fabrication of ferromagnetic contacts by electron beam lithography and electron beam evaporation of metals (1 nm TiO$_2$/65 nm Co). The magnetic field sweeps at different temperatures were carried out in a Quantum Design Physical Property Measurement System while electrical biases were applied and measured by an external Keithley 6221 current source and a Keithley 2182A nanovoltmeter, respectively.

DFT simulations
For calculation of the electronic structure and structural relaxation of graphene on CGT density functional theory (DFT) [46] was used within Quantum ESPRESSO [47] using a previously developed model ([31]) with a k-point sampling of $6 \times 6 \times 1$, a Hubbard parameter of $U = 1$ eV [17], an energy cutoff for charge density of 500 Ry, and a

kinetic energy cutoff for wave functions of 60 Ry [48, 49]. When SOC is included, we used the relativistic versions of the pseudopotentials. For the relaxation of the heterostructures, we added van der Waals corrections [50, 51] and used a quasi-Newton algorithm based on a trust radius procedure. A vacuum gap of 20 Å was used to simulate quasi-2D systems. To determine the interlayer distances, the atoms of graphene were allowed to relax only in z direction (vertical to the layers) for determination of the interlayer distances, while the atoms of CGT were free to move in all directions until reaching a state when all components of all forces were reduced below 10^{-3} [Ry/a_0] (a_0 is the Bohr radius). For more details, see [31].

Acknowledgments

Contributions

SPD and BK conceived the idea and designed the experiments. BK fabricated and measured the devices. AWC, MV, SR performed the simulations. KZ and JF performed the theoretical calculations. DK, AMH, AD helped in device fabrication and measurements. PS performed SQUID magnetic characterization of bulk CGT crystal. BK, AWC, MV, KZ, JF, SR, SPD contributed in analysis of the data, compiled the figures and wrote the manuscript. All authors gave input on interpretation of the data and contributed in writing of the manuscript. SPD supervised and managed the project.

Competing interests

The authors declare no competing financial interests.

ORCID iDs

Bogdan Karpiak ⬤ https://orcid.org/0000-0001-7462-8405
Aron W Cummings ⬤ https://orcid.org/0000-0003-2307-497X
Klaus Zollner ⬤ https://orcid.org/0000-0002-6239-3271
Marc Vila ⬤ https://orcid.org/0000-0001-9118-421X
Dmitrii Khokhriakov ⬤ https://orcid.org/0000-0002-5515-9081
Anamul Md Hoque ⬤ https://orcid.org/0000-0002-2117-7177
Peter Svedlindh ⬤ https://orcid.org/0000-0002-3049-6831
Stephan Roche ⬤ https://orcid.org/0000-0003-0323-4665
Saroj P Dash ⬤ https://orcid.org/0000-0001-7931-4843

References

[1] Wang J and Zhang S-C 2017 Topological states of condensed matter *Nat. Mater.* **16** 1062–7
[2] He Q L *et al* 2017 Chiral Majorana fermion modes in a quantum anomalous Hall insulator–superconductor structure *Science* **357** 294–9
[3] Qiao Z *et al* 2014 Quantum anomalous Hall effect in graphene proximity coupled to an antiferromagnetic insulator *Phys. Rev. Lett.* **112** 116404
[4] Qiao Z *et al* 2010 Quantum anomalous Hall effect in graphene from rashba and exchange effects *Phys. Rev.* B **82** 161414
[5] Roche S *et al* 2015 Graphene spintronics: the European Flagship perspective *2D Mater.* **2** 030202
[6] Yang H X *et al* 2013 Proximity effects induced in graphene by magnetic insulators : first-principles calculations on spin filtering and exchange-splitting gaps *Phys. Rev. Lett.* **110** 046603
[7] Hallal A, Ibrahim F, Yang H, Roche S and Chshiev M 2017 Tailoring magnetic insulator proximity effects in graphene: first-principles calculations *2D Mater.* **4** 025074
[8] Zhong D *et al* 2017 Van der Waals engineering of ferromagnetic semiconductor heterostructures for spin and valleytronics *Sci. Adv.* **3** e1603113
[9] Haugen H, Huertas-Hernando D and Brataas A 2008 Spin transport in proximity-induced ferromagnetic graphene *Phys. Rev.* B **77** 115406
[10] Yang H *et al* 2018 Significant Dzyaloshinskii-Moriya interaction at graphene-ferromagnet interfaces due to Rashba effect *Nat. Mater.* **17** 605–9
[11] Dyrdał A and Barnaś J 2017 Anomalous, spin, and valley Hall effects in graphene deposited on ferromagnetic substrates *2D Mater.* **4** 034003
[12] Wang Z, Tang C, Sachs R, Barlas Y and Shi J 2015 Proximity-induced ferromagnetism in graphene revealed by the anomalous Hall effect *Phys. Rev. Lett.* **114** 016603
[13] Tang C *et al* 2018 Approaching quantum anomalous Hall effect in proximity-coupled YIG/graphene/h-BN sandwich structure *APL Mater.* **6** 026401
[14] Wei P *et al* 2016 Strong interfacial exchange field in the graphene/EuS heterostructure *Nat. Mater.* **15** 711–6
[15] Singh S *et al* 2017 Strong modulation of spin currents in bilayer graphene by static and fluctuating proximity exchange fields *Phys. Rev. Lett.* **118** 187201
[16] Leutenantsmeyer J C, Kaverzin A A, Wojtaszek M and Van Wees B J 2017 Proximity induced room temperature

ferromagnetism in graphene probed with spin currents *2D Mater.* **4** 014001

[17] Gong C *et al* 2017 Discovery of intrinsic ferromagnetism in two-dimensional van der Waals crystals *Nature* **546** 265–9

[18] Huang B *et al* 2017 Layer-dependent ferromagnetism in a van der Waals crystal down to the monolayer limit *Nature* **546** 270–3

[19] Tan C *et al* 2018 Hard magnetic properties in nanoflake van der Waals Fe_3GeTe_2 *Nat. Commun.* **9** 1554

[20] Wang Z *et al* 2018 Electric-field control of magnetism in a few-layered van der Waals ferromagnetic semiconductor *Nat. Nanotechnol.* **13** 554–9

[21] Huang B *et al* 2018 Electrical control of 2D magnetism in bilayer CrI_3 *Nat. Nanotechnol.* **13** 544–8

[22] Jiang S, Li L, Wang Z, Mak K F and Shan J 2018 Controlling magnetism in 2D CrI_3 by electrostatic doping *Nat. Nanotechnol.* **13** 549–53

[23] Klein D R *et al* 2018 Probing magnetism in 2D van der Waals crystalline insulators via electron tunneling *Science* **360** 1218–22

[24] Song T *et al* 2018 Giant tunneling magnetoresistance in spin-filter van der Waals heterostructures *Science* **360** 1214–8

[25] Wang Z *et al* 2018 Very large tunneling magnetoresistance in layered magnetic semiconductor CrI_3 *Nat. Commun.* **9** 2516

[26] Wang Z *et al* 2018 Tunneling spin valves based on Fe_3GeTe_2/hBN/Fe_3GeTe_2 van der Waals Heterostructures *Nano Lett.* **18** 4303–8

[27] Ghazaryan D *et al* 2018 Magnon-assisted tunnelling in van der Waals heterostructures based on $CrBr_3$ *Nat. Electron.* **1** 344–9

[28] Alegria L D *et al* 2014 Large anomalous Hall effect in ferromagnetic insulator-topological insulator heterostructures *Appl. Phys. Lett.* **105** 1–5

[29] Wu Y *et al* 2019 Néel-type skyrmion in WTe_2/Fe_3GeTe_2 van der Waals heterostructure (arXiv:1907.11349)

[30] Zhang J, Zhao B, Yao Y and Yang Z 2015 Robust quantum anomalous Hall effect in graphene-based van der Waals heterostructures *Phys. Rev.* B **92** 165418

[31] Zollner K, Gmitra M and Fabian J 2018 Electrically tunable exchange splitting in bilayer graphene on monolayer $Cr_2X_2Te_6$ with X = Ge, Si, and Sn *New J. Phys.* **20** 073007

[32] Zhang J *et al* 2017 Strong magnetization and Chern insulators in compressed graphene/CrI_3 van der Waals heterostructures *Phys. Rev.* B **97** 085401

[33] Xing W *et al* 2017 Electric field effect in multilayer $Cr_2Ge_2Te_6$: a ferromagnetic 2D material *2D Mater.* **4** 024009

[34] Carteaux V, Brunet D, Ouvrard G and André G 1995 Crystallographic, magnetic and electronic structures of a new layered ferromagnetic compound $Cr_2Ge_2Te_6$ *J. Phys.: Condens. Matter* **7** 69–87

[35] Li X and Yang J 2014 $CrXTe_3$ (X = Si, Ge) nanosheets: two dimensional intrinsic ferromagnetic semiconductors *J. Mater. Chem.* C **2** 7071–6

[36] Tian Y, Gray M J, Ji H, Cava R J and Burch K S 2016 Magneto-elastic coupling in a potential ferromagnetic 2D atomic crystal *2D Mater.* **3** 025035

[37] Ferrari A, Meyer J C, Scardaci C, Casiraghi C and Lazzeri M 2006 Raman spectrum of graphene and graphene layers *Phys. Rev. Lett.* **97** 187401

[38] Kamalakar V M, Groenveld C, Dankert A and Dash S P 2015 Long distance spin communication in chemical vapour deposited graphene *Nat. Commun.* **6** 6766

[39] Cummings A W 2019 Probing magnetism via spin dynamics in graphene/2D-ferromagnet heterostructures *J. Phys. Mater.* **2** 045007

[40] Hahn E L and Abragam A 1992 *Pulsed Magnetic Resonance: NMR, ESR, and Optics* (Oxford: Clarendon)

[41] Fabian J, Matos-Abiaguea A, Ertlera C, Stano P and Zutic I 2007 Semiconductor spintronics *Acta Phys. Slovaca* **57** 565–907

[42] Ringer S *et al* 2018 Measuring anisotropic spin relaxation in graphene *Phys. Rev.* B **97** 205439

[43] Raes B *et al* 2016 Determination of the spin-lifetime anisotropy in graphene using oblique spin precession *Nat. Commun.* **7** 11444

[44] Cummings A W, Garcia J H, Fabian J and Roche S 2017 Giant spin lifetime anisotropy in graphene induced by proximity effects *Phys. Rev. Lett.* **119** 206601

[45] Garcia J H, Vila M, Cummings A W and Roche S 2018 Spin transport in graphene/transition metal dichalcogenide heterostructures *Chem. Soc. Rev.* **47** 3359–79

[46] Honenberg P and Kohn W 1964 Inhomogeneous electron gas *Phys. Rev.* **136** B864–71

[47] Giannozzi P *et al* 2009 QUANTUM ESPRESSO : a modular and open-source software project for quantum simulations of materials *J. Phys.: Condens. Matter* **21** 395502

[48] Kresse G and Joubert D 1999 From ultrasoft pseudopotentials to the projector augmented-wave method *Phys. Rev.* B **59** 1758–75

[49] Perdew J P, Burke K and Ernzerhof M 1996 Generalized gradient approximation made simple *Phys. Rev. Lett.* **77** 3865–8

[50] Grimme S 2006 Semiempirical GGA-type density functional constructed with a long-range dispersion correction *J. Comput. Chem.* **27** 1787–99

[51] Barone V *et al* 2008 Role and effective treatment of dispersive forces in materials : polyethylene and graphite crystals as test cases *J. Comput. Chem.* **30** 934–9